Entropy Generation in a Magnetohydrodynamic Hybrid Nanofluid Flow over a Nonlinear Permeable Surface with Velocity Slip Effect

S. O. SALAWU[1], H. A. OGUNSEYE[2], T. A. YUSUF[3], R. S. LEBELO[4], R. A. MUSTAPHA[5]
[1]Department of Mathematics,
Bowen University,
Iwo,
NIGERIA

[2]West Virginia Academy,
Al Wukair, Doha,
QATAR

[3]Department of Mathematics,
Adeleke University,
Ede,
NIGERIA

[4]Education Department,
Vaal University of Technology,
Vanderbijlpark,
SOUTH AFRICA

[5]Department of Mathematics,
Lagos State University,
Lagos,
NIGERIA

Abstract: - The current study is designed to model the hydrothermal feature of a hybrid nano liquid slip flows over a permeable expanding/contracting surface with entropy generation. The model incorporates Cu-Al_2O_3 nanoparticles with water as the host liquid to simulate the flow. Additional impacts incorporated into the novelty of the model are viscous dissipation and Joule heating. The model is transformed appropriately to its dimensionless form using similarity quantities and the solution is numerically obtained using the spectral quasi-linearization method (SQLM). The impact of pertinent factors on the flow characteristics is communicated through graphs for the hybrid nano-suspension to discuss the hydrothermal variations. The friction factor and the rate of heat transport are also discussed with sensible judgment through tables. To ensure the code validity, a comparison with earlier studies is conducted and excellent consensus is accomplished. The result explored that diminution in the irreversibility ratio is witnessed for rising magnetic field strength along the free stream, distance away from the permeable surface as the heat dissipation to the surrounding decelerates. Also, the augmented nonlinearity parameter intensified the heat transfer rate for about 2.79% of the hybrid nano-suspension.

Key-Words: - Boundary slip; entropy generation; Magnetohydrodynamic; hybrid nanofluid; nonlinear permeable surface

Received: October 15, 2022. Revised: May 18, 2023. Accepted: June 19, 2023. Published: July 27, 2023.

1 Introduction

Fluid flows over stretching or shrinking surfaces are extremely noteworthy owing to their wide range of applications. Different aspects of fluid flow overstretched surfaces under various flow conditions can be traced out through the open pieces of literature, [1], [2], [3], [4]. Since the innovative research articles have devoted interest to the field of flow through a stretching surface. However, the blowing (suction) or withdrawal (injection) phenomena associated with fluid flow over a stretched surface have a tremendous impact on the flow field. It has useful engineering applications in the design of thrust bearings and radial diffusers to prevent corrosion and thermal oil recovery. In, [5], the authors discussed the suction/injection effect on a boundary layer flow due to stretching the surface with thermal radiation. The author claimed that the injection tends to eclipse skin friction, while the suction acts otherwise. Convection flows over a stretching or shrinking surface with suction or injection is numerically investigated by, [6]. Some recent related articles are, [7], [8], [9]. In, [10], the author discussed the Darcy-Forchheimer flow of nanofluid through a stretchy, permeable wall. It was found that the flow rate decreases with rising Darcy-Forchheimer numbers.

Some common liquids like water, mineral oils, and ethylene glycol, are found to have low thermal characteristics when compared with metals, non-metals, and their oxides. Researchers have in the past years come up with the notion of the suspension of millimeter-sized solid material in a liquid, [11]. However, when these suspended particles are larger, a lot of technical issues are encountered, including an increasing drop in pressure, erosion of pipelines, etc. Given these challenges, the idea of improving thermal conductivity by employing nano-sized materials was later coined by, [12]. The author experimentally analyzed the enhancement of thermal conductivity through the dispersion of nanoparticles in conventional-based liquids named nanofluids. Other than improving thermal conductivity, the choice of adding nano-sized materials over micro-sized particles inside a conventional base fluid has been a promising candidate due to several valid scientific reasons, such as shape, size, concentration, wide suspension time (more stability), and significant energy savings, [13]. In, [14], carried out a comparative analysis on the viscous fluid of different nanoparticles in a rotating slip disk and Joule heating. A high-volume fraction of nanoparticles dampened the axial velocity. In terms of provision of efficient heat transfer and coolant issues, a modified version of nanofluid i.e. hybrid nanofluid, has recently been introduced and has significant uses in pharmaceutical medicine, electronics, chemical industry, agriculture, and so on, [15]. In the hybrid nanofluid, two or more metallic nanoparticles are dispersed within the base fluid. In, [16], the authors examined the influence of heat transfer enhancement and thermal conductivity in hybrid nanofluids of water-based suspended Cu-Al_2O_3 over a stretched surface using a numerical approach. In, [17], the authors used the concept of a hybrid nanofluid of Ag-CuO water-based to communicate the analysis of 3D flow, heat, and mass transfer of a rotating liquid past a stretching sheet. They reported through their analysis that hybridity is boosted by enhancing the heat transfer rate at the surface. Recently, a semi-analytical method was employed to examine the 3-D flow of a water-based hybrid nanofluid over a stretched surface with Darcy-Forchheimer porous medium and nonlinear thermal radiation by, [18], [19], discussed the inclined magnetic field effect on hybrid nanofluid flow over a slip surface. They explore Silver and copper oxide nanoparticles as hybrid nanofluids, while copper oxide is the usual nanofluid with base fluid water. They claim that maximum heat transfer capability is noticed for the hybrid nanofluid when compared with the ordinary nanofluid. In, [20], the authors numerically studied a 2-D steady flow with the analysis of heat transfer of water-based Cu-Al_2O_3 nanoparticles over a permeable stretching sheet with thermal radiation.

Entropy generation, a noteworthy function in thermal engineering, is often affected mainly due to conduction, and convection within the system. The analysis of entropy generation has snatched the attention of so many researchers globally as it helps to control the irreversibility losses in a thermal system that may affect system efficiency, [21]. It is a pertinent factor, particularly in the industries and engineering processes where cooling and heating procedures are fostered. The result of an irreversible process that takes place in homogeneous thermodynamic systems can be linked to thermal dissipation and Joule heating. These are significant in examining the level of entropy generated in a thermal system. In an attempt to obtain an optimum design criterion, investigation in this direction by several authors over diverse flow geometries can be found in references, [22], [23]. In, [24], the authors

examined the Arrhenius kinetics of thermal diffusion of nano liquid squeezing second-grade fluid flow along an infinite plate and entropy generation. As seen, the Brinkman number discouraged the rate of generation of entropy. Meanwhile, great improvements have been reported for hybrid nanofluids over conventional fluids in the analysis of entropy generation. For instance, In, [25], the authors studied the entropy generation analysis of water-Fe_3O_4/CNT hybrid nanofluid flow inside a concentric horizontal annulus using a numerical approach. Furthermore, In, [22], the authors examine a steady flow of hybrid nanofluid with entropy generation by including melting heat transfer to address the heat transfer analysis. They concluded that the irreversibility ratio is lower for hybrids as compared to the usual nanofluid. In, [26], the authors numerically examine the entropy generation characteristics of a water-based hybrid nanofluid flow over a slippery wedge surface with variable viscosity. They reported that increasing the volume fraction of nanoparticles eclipse the entropy production. For further results on the entropy generation in hybrid nanofluid, interested readers can see the following references, [27], [28], [29].

Inspired by the above research, we have presented in this communication the impacts of the water-based Cu-Al_2O_3 hybrid nano liquid flowing through a permeable stretching surface. The analysis of entropy generation is included to explore the flow and heat interaction. With many studies on hybrid nanofluids, no mathematical post of the present study has been done subject to the boundary conditions. Despite several solution techniques, [2], [20], in handling nonlinear ODEs, resulting equations from this present study were solved using the spectral quasi-linearization method (SQLM) owning to its rapid convergence, [30], [31]. The outcomes convey the impacts for both hybrid and usual nanofluids. The study objectives are to examine the: velocity, temperature, and rate of entropy generation, and the Bejan figures are captured to have requisite information on the flow and heat transfer. Skin friction and Nusselt number are also reported via Table. To the best of our knowledge, no investigation on the mentioned issues has so far been reported. Thus, we hope that this study will provide a basis to gather the indispensable information of such flow which in turn helps various technological issues.

2 Problem Formulation

We consider a steady 2-D flow of a two-dimensional non-linearly stretching permeable sheet with velocity slip and prescribed surface heat flux with the working fluid being an electrically conducting viscous hybrid nanofluid. The permeable sheet is stretching with assumed velocity $u_w(x) = ax^m$ also, the external velocity takes $u_e = cx^m$, where a and c are positive constants. Here, $m \neq 1$ is the nonlinearity parameter. A non-uniform magnetic field acts normally to the flow direction with strength $B(x) = B_0 x^{(m-1)/2}$, where B_0 is the applied magnetic field strength as geometrically modeled in Figure 1.

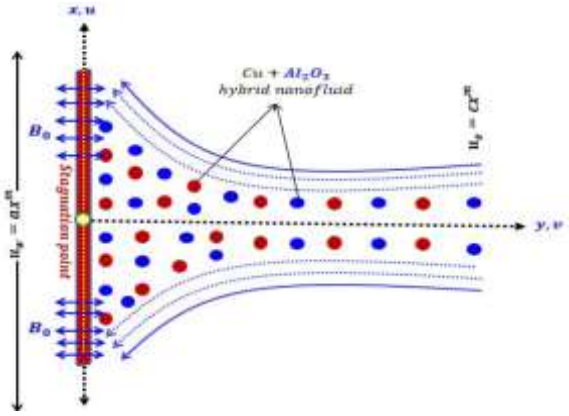

Fig. 1: The theoretical physical model

Using the boundary layer approximations and accounting for the impacts of Joule heating and viscous dissipation, the hybrid nanofluid model equations are [2], [20]:

$$\frac{\partial u}{\partial x} + \frac{\partial v}{\partial y} = 0 \tag{1}$$

$$u\frac{\partial u}{\partial x} + v\frac{\partial u}{\partial y} = u_e\frac{du_e}{dx} + \frac{\mu_{hnf}}{\rho_{hnf}}\frac{\partial^2 u}{\partial y^2} + \frac{\sigma_{hnf}B(x)^2}{\rho_{hnf}}(u_e - u), \tag{2}$$

$$u\frac{\partial T}{\partial x} + v\frac{\partial T}{\partial y} = \frac{k_{hnf}}{(\rho C_p)_{hnf}}\frac{\partial^2 T}{\partial y^2} + \frac{\mu_{hnf}}{(\rho C_p)_{hnf}}\left(\frac{\partial u}{\partial y}\right)^2 + \frac{\sigma_{hnf}B(x)^2}{(\rho C_p)_{hnf}}(u - u_e)^2 \tag{3}$$

and at the boundary, the model is set as:

$$u = u_w + \lambda(x)\frac{\mu_{hnf}}{\rho_{hnf}}\frac{\partial u}{\partial y}, \quad v = v_w, \quad T = T_w(T_\infty + Ax^r), \quad \text{at} \quad y = 0, \tag{4}$$

$$u \longrightarrow u_e(x), \quad T \longrightarrow T_\infty, \quad \text{as} \quad y \longrightarrow \infty. \tag{5}$$

Here, the hybrid nanofluid dynamic viscosity, density, electrical conductivity, thermal conductivity, and heat capacity represent μ_{hnf}, ρ_{hnf}, σ_{hnf}, k_{hnf} and $(\rho C_p)_{hnf}$ respectively. x represent the coordinate along the surface and the vertical coordinate takes y, u and v respectively represent a component of the velocity along x and y directions, T is the hybrid nanofluid temperature, σ_v is the tangential momentum accommodation coefficient, $\lambda(x) = \lambda_0 x^{(m-1)/2}$ is the mean free path, v_w is the suction (injection) velocity, T_w is the wall temperature, and r is the surface temperature parameter. In addition, the expression to evaluate these thermo-physical properties for both nanofluid and hybrid nanofluid is presented in Table 1, where, the subscript nf denotes the nanofluid, f indicates the base fluid, hnf indicates the hybrid nanofluid, while n_1 and n_2 represents the hybrid nanoparticles. In this model, water is considered as a base fluid and Cu-Al_2O_3 is considered due to the thermal conductivity and heat convective strength of the nanoparticles and the base fluid. This is synthesized by dissipating a fraction of Al_2O_3 (φ_{n_1}) nanoparticle to water (base fluid).

Table 1. Thermo-physical properties of nanofluid and hybrid nanofluid

Property	Nanofluid	Hybrid Nanofluid
Dynamic viscosity	$\mu_{nf} = \frac{\mu_f}{(1-\varphi_{n_1})^{2.5}}$	$\mu_{hnf} = \frac{\mu_f}{(1-\varphi_{n_1})^{2.5}(1-\varphi_{n_2})^{2.5}}$
Density	$\rho_{nf} = (1-\varphi_{n_1})\rho_f + \varphi_{n_1}\rho_{n_1}$	$\rho_{hnf} = (1-\varphi_{n_2})[(1-\varphi_{n_1})\rho_f + \varphi_{n_1}\rho_{n_1}] + \varphi_{n_2}\rho_{n_2}$
Electrical conductivity	$\sigma_{nf} = 1 + \frac{3\left(\frac{\sigma_{n_1}}{\sigma_f}-1\right)\varphi_{n_1}}{2+\frac{\sigma_{n_1}}{\sigma_f}-\left(\frac{\sigma_{n_1}}{\sigma_f}-1\right)\varphi_{n_1}} \times \sigma_f$	$\sigma_{hnf} = \frac{\sigma_{n_2}+2\sigma_{nf}-2\varphi_{n_2}(\sigma_{nf}-\sigma_{n_2})}{\sigma_{n_2}+2\sigma_{nf}+\varphi_{n_2}(\sigma_{nf}-\sigma_{n_2})} \times \sigma_{nf}$ where $\sigma_{nf} = \frac{\sigma_{n_1}+2\sigma_f-2\varphi_{n_1}(\sigma_f-\sigma_{n_1})}{\sigma_{n_1}+2\sigma_f+\varphi_{n_1}(\sigma_f-\sigma_{n_1})} \times \sigma_f$
Thermal conductivity	$k_{nf} = \frac{k_{n_1}+2k_f-2\varphi_{n_1}(k_f-k_{n_1})}{k_{n_1}+2k_f+\varphi_{n_1}(k_f-k_{n_1})} \times k_f$	$k_{hnf} = \frac{k_{n_2}+2k_{nf}-2\varphi_{n_2}(k_{nf}-k_{n_2})}{k_{n_2}+2k_{nf}+\varphi_{n_2}(k_{nf}-k_{n_2})} \times k_{nf}$ where $k_{nf} = \frac{k_{n_1}+2k_f-2\varphi_{n_1}(k_f-k_{n_1})}{k_{n_1}+2k_f+\varphi_{n_1}(k_f-k_{n_1})} \times k_f$
Heat capacity	$(\rho C_p)_{nf} = (1-\varphi_{n_1})(\rho C_p)_f + \varphi_{n_1}(\rho C_p)_{n_1}$	$(\rho C_p)_{hnf} = (1-\varphi_{n_2})\left[(1-\varphi_{n_1})(\rho C_p)_f + \varphi_{n_1}(\rho C_p)_{n_1}\right] + \varphi_{n_2}(\rho C_p)_{n_2}$

Source: [16], [17], [20]

Different volume fractions of Cu(φ_{n_2}) are subsequently added. It is interesting to note that, for $\varphi_{n_1} = \varphi_{n_2} = 0$, a working fluid (water) is retrieved. More so, when $\varphi_{n_1} = 0$ and $\varphi_{n_2} \neq 0$, a case of Cu/water nanofluid can be obtained. The thermo-physical features of water and the hybrid nanoparticles are presented in Table 2.

Table 2. Thermo-physical properties of ethylene glycol and hybrid nanoparticles

	ρ	C_p	k	σ
	kg/m^3	J/kgK	W/mK	Sm
Water	997.1	4 179	0.613	0.05
Cu	8933	385	400	5.96×10^7
Al_2O_3	3970	765	40	3.69×10^7

Source: [20]

With aid of the below transformation ([4], [20]):

$$\eta = \left(\frac{a}{\nu_f}\right)^{1/2} x^{(m+1)/2} y, \quad \theta(\eta) = \frac{T-T_\infty}{T_w-T_\infty}, \quad \psi = (a\nu_f)^{1/2} x^{(m+1)/2} f(\eta), \tag{5}$$

here, $u = \partial\psi/\partial y$ and $v = -\partial\psi/\partial x$, where ψ represents the stream function, also ν_f represent the kinematic viscosity of the base fluid. Also, to obtain a similar solution, $q_w(x)$ and $v_w(x)$ are defined according to [1], as:

$$v_w(x) = -\frac{(a\nu_f)^{\frac{1}{2}}(m+1)}{2} x^{\frac{m-1}{2}} S \quad \text{and} \quad r = 2m, \tag{6}$$

$S = f(0)$ denotes the constant mass flux parameter with $S > 0$ signifying fluid suction and $S < 0$ depicts fluid injection. Substituting equations (5,6) into equations (1-4) yields:

$$\frac{A_1}{A_2} f''' + \frac{m+1}{2} f f'' + m\left(1 - f'^2\right) - \frac{A_3}{A_2} M(f' - 1) = 0 \tag{7}$$

$$\frac{1}{Pr}\frac{A_4}{A_5}\theta'' + \frac{(m+1)}{2} f\theta' - 2mf'\theta + \frac{Ec}{A_5}[A_1 f''^2 + A_3 M(f'-1)^2] = 0, \tag{8}$$

subjected to:

$$f(0) = S, \quad f'(0) = \varepsilon + \delta\frac{A_1}{A_2} f''(0), \quad \theta(0) = 1, \tag{9}$$

$$f'(\eta) \longrightarrow 1, \quad \theta(\eta) \longrightarrow 0 \quad \text{as} \quad \eta \longrightarrow \infty, \tag{10}$$

where the magnetic parameter M, Prandtl number Pr, Eckert number Ec, velocity slip parameter, and the velocity ratio parameter are defined as:

$$\left.\begin{gathered} M=\frac{\sigma_f B_0^2}{a\rho_f},\quad Pr=\frac{(\mu C_p)_f}{k_f},\quad Ec=\frac{a^2}{AC_{p_f}},\quad \varepsilon=\frac{c}{a},\\ \delta=\lambda_0\sqrt{a\nu_f}\,A_1=\frac{\mu_{hnf}}{\mu_f},\quad A_2=\frac{\rho_{hnf}}{\rho_f},\quad A_3=\frac{\sigma_{hnf}}{\sigma_f},\\ A_4=\frac{k_{hnf}}{k_f},\quad A_5=\frac{(\rho C_p)_{hnf}}{(\rho C_p)_f}, \end{gathered}\right\} \tag{11}$$

The relevant quantities of engineering interest in this work and their corresponding mathematical descriptions of the skin friction coefficient C_{fx} and the Nusselt number Nu_x are portrayed as:

$$C_{fx}=\frac{\tau_w(x)}{\rho_f u_e^2},\qquad Nu_x=\frac{xq_w(x)}{k_f(T_w-T_\infty)}, \tag{12}$$

where $\tau_w(x)=\mu_{hnf}(\partial u/\partial y)_{y=0}$ denotes the surface shear stress and $q_w(x)=-k_{hnf}(\partial T/\partial y)_{y=0}$ represents the wall heat flux. Using equation (5), equation (12) is gotten as follows:

$$Re_x^{1/2}C_f=A_1f''(0),Re_x^{-1/2}Nu_x=-A_4\theta'(0) \tag{13}$$

where the local Reynolds number $Re_x=\frac{u_e x}{\nu_f}$.

2.1 Entropy Generation

Based on the second law of thermodynamics, the analysis of entropy generation for the present study is portrayed as, [9],

$$S'''_{\text{gen}}=\frac{k_{hnf}}{T_\infty^2}\left(\frac{\partial T}{\partial y}\right)^2+\frac{\mu_{hnf}}{T_\infty}\left(\frac{\partial u}{\partial y}\right)^2+\frac{\sigma_{hnf}}{T_\infty}B_0^2(x)(u-u_e)^2 \tag{14}$$

Using the dimensionless variable defined above in equation (5), the entropy generation number can be rewritten as:

$$Ns=A_4\theta'^2+\frac{EcPr}{\Omega}[A_1f''^2+A_3M(f'-1)^2] \tag{15}$$

where $\Omega=\frac{T_w-T_\infty}{T_\infty}$ is the temperature difference parameter.

The Bejan number (Be) is defined as

$$Be=\frac{A_4\theta'^2}{A_4\theta'^2+\frac{EcPr}{\Omega}[A_1f''^2+A_3M(f'-1)^2]}, \tag{16}$$

3 Numerical Solution

The analytical solutions to the boundary value problem given by equations (7-10) are nearly impossible to obtain, for these equations are highly nonlinear, hence, we resolve a numerical method. The solution is therefore obtained via the spectral quasi-linearization method (SQLM). The employed numerical technique was adopted for this study because it is found to be stable, consistent, and convergence. This method is employed to numerically integrate the coupled nonlinear differential equations (7-10). Recently, SQLM has been shown to be efficient in solving nonlinear boundary value problems emerging from boundary layer flow, in terms of accuracy and rapid convergence, [30], [31].

To apply the SQLM, the following non-linear differential operators are considered:

$$\Phi_f=\frac{A_1}{A_2}f_{n'''}+\frac{m+1}{2}f_nf_{n''}+m(1-f_{n'}^2)-\frac{A_3}{A_2}M(f_{n'}-1), \tag{17}$$

$$\Phi_\theta=\frac{1}{Pr}\frac{A_4}{A_5}\theta_{n''}+\frac{(m+1)}{2}f_n\theta_{n'}-2mf_{n'}\theta_n+\frac{Ec}{A_5}[A_1f_{n''}^2+A_3M(1-f_{n'})^2]. \tag{18}$$

With respect to SQLM, equations (7,8) are linearized using the Newton-Raphson algorithm as described by, [32], to give the following iterative scheme:

$$a_{1,r}f'''_{r+1}+a_{2,r}f''_{r+1}+a_{3,r}f'_{r+1}+a_{4,r}f_{r+1}=R_r^f, \tag{19}$$

$$a_{5,r}\theta''_{r+1}+a_{6,r}\theta'_{r+1}+a_{7,r}\theta_{r+1}+a_{8,r}f''_{r+1}+a_{9,r}f'_{r+1}+a_{10,r}f_{r+1}=R_r^\theta, \tag{20}$$

subject to the corresponding boundary conditions:

$$f'_{n+1}(0)-\delta\frac{A_1}{A_2}f''_{n+1}(0)=\varepsilon,f_{n+1}(0)=S,f'_{n+1}(\infty)=1,\theta_{n+1}(0)=1,\theta_{n+1}(\infty)=0 \tag{21}$$

where the coefficients $a_{i,n}$ $(i=1,\dots,10)$, are defined as:

$$\left.\begin{gathered} a_{1,n}=\frac{\partial\Phi_f}{\partial f_{r'''}},\quad a_{2,n}=\frac{\partial\Phi_f}{\partial f_{r''}},\quad a_{3,n}=\frac{\partial\Phi_f}{\partial f_{r'}},\\ a_{4,n}=\frac{\partial\Phi_f}{\partial f_r},\quad a_{5,n}=\frac{\partial\Phi_\theta}{\partial\theta'_r},\\ a_{6,n}=\frac{\partial\Phi_\theta}{\partial\theta'_r},\quad a_{7,n}=\frac{\partial\Phi_\theta}{\partial\theta_r},\quad a_{8,n}=\frac{\partial\Phi_\theta}{\partial f''_r},\\ a_{9,n}=\frac{\partial\Phi_\theta}{\partial f'_r},\quad a_{10,n}=\frac{\partial\Phi_\theta}{\partial f_r} \end{gathered}\right\} \tag{22}$$

and

$$\left.\begin{gathered} R_r^f=a_{1,r}f_r'''+a_{2,r}f_r''+a_{3,r}f_r'+a_{4,r}f_r-\Phi_f,\\ R_r^\theta=a_{5,r}\theta_r''+a_{6,r}\theta_r'+a_{7,r}\theta_n+a_{8,n}f_n''+a_{9,n}f_n'\\ +a_{8,n}f_n''+a_{9,n}f_n'a_{10,n}f_n-\Phi_\theta \end{gathered}\right\} \tag{23}$$

The SQLM iterative scheme which is made up of equations (19-21) is solved numerically with the aid of the Chebyshev pseudo-spectral scheme. Equations (19, 20) are discretized with the help of this scheme. Furthermore, using the transformation $\eta = \frac{1}{2}(\pi + 1)\varpi_\infty$, to transform the interval $[0, \varpi_\infty] \mapsto [-1,1]$. Then, the semi-infinite domain, $\eta \in [0, \infty)$ is truncated by replacing it with the domain $\eta \in [0, \varpi_\infty]$, where $\varpi_\infty \in \mathbb{Z}^+$.

The computation of $f(\eta)$ and $\theta(\eta)$ (i.e the derivatives of the unknown variables) is done using the Chebyshev differentiation matrix D, [33], at the collocation points as a matrix-vector product;

$$\frac{df}{d\eta} = \sum_{i=0}^{\bar{N}} D_{ij} f(\pi_i) = \mathbf{D}F, \quad j = 0,1,2,\dots,\bar{N}, \tag{24}$$

$$\frac{d\theta}{d\eta} = \sum_{i=0}^{\bar{N}} D_{ij} \theta(\pi_i) = \mathbf{D}\Theta, \quad j = 0,1,2,\dots,\bar{N}, \tag{25}$$

where $\bar{N}$ denotes the number of collocation points, $\mathbf{D} = 2D/\varpi_\infty$, $F = [f(\pi_0), f(\pi_1), \dots, f(\pi_{\bar{N}})]^T$ and $\Theta = [\theta(\pi_0), \theta(\pi_1), \dots, \theta(\pi_{\bar{N}})]^T$ are vector functions at the collocation point.

The Gauss-Lobatto points are chosen to define the nodes in $[-1,1]$ as:

$$\pi_k = \cos\left(\frac{\pi k}{\bar{N}}\right), \quad k = 0,1,\dots,\bar{N}; \quad -1 \le \pi \le 1. \tag{26}$$

Higher order derivatives of f and θ are evaluated as powers of $\mathbf{D}$, that is

$$f^s(\eta) = \mathbf{D}^s F, \quad \text{and} \quad \theta^s(\eta) = \mathbf{D}^s \Theta. \tag{27}$$

Substituting Eqs. (24) – (27) into Eqs. (19) – (21), we obtain the following matrix form:

$$\begin{bmatrix} H_{11} & H_{12} \\ H_{21} & H_{22} \end{bmatrix} \begin{bmatrix} F_{r+1} \\ \Theta_{r+1} \end{bmatrix} = \begin{bmatrix} R_r^f \\ R_r^\theta \end{bmatrix} \tag{28}$$

where H_{ij} $(i,j = 1,\dots,2)$ are $(\bar{N}+1) \times (\bar{N}+1)$ matrices and R_n^f and R_n^θ are $(\bar{N}+1) \times 1$ vectors, such that:

$$\left.\begin{aligned} H_{11} &= \mathrm{diag}[a_{1,r}]\mathbf{D}^3 + \mathrm{diag}[a_{2,r}]\mathbf{D}^2 \\ &\quad + \mathrm{diag}[a_{3,r}]\mathbf{D} + \mathrm{diag}[a_{4,r}]\mathbf{I}, \\ H_{12} &= 0_{\bar{N}+1 \times \bar{N}+1} \\ H_{21} &= \mathrm{diag}[\alpha_{8,r}]\mathbf{D}^2 + \mathrm{diag}[\alpha_{9,r}]\mathbf{D} \\ &\quad + \mathrm{diag}[\alpha_{10,r}]\mathbf{I}, \quad H_{22} = \mathrm{diag}[\alpha_{5,r}]\mathbf{D}^2 \\ &\quad + \mathrm{diag}[\alpha_{6,r}]\mathbf{D} + \mathrm{diag}[\alpha_{7,r}]\mathbf{I} \end{aligned}\right\} \tag{29}$$

subject to the boundary conditions

$$\left.\begin{aligned} F_{n+1}(\pi_{\bar{N}}) = S, \sum_{i=0}^{\bar{N}} \left[\mathbf{D}_{\bar{N}i} - \delta \frac{A_1}{A_2} \mathbf{D}_{\bar{N}i}^2\right] F_{r+1}(\pi_{\bar{N}}) = \varepsilon, \\ \Theta_{r+1}(\pi_{\bar{N}}) = 1, \quad \Theta_{r+1}(\pi_0) = 0 \end{aligned}\right\} \tag{30}$$

The SQLM scheme is initialized with the following initial approximation;

$$\left.\begin{aligned} \theta_0(\eta) &= \exp(-\eta) \quad \text{and} \\ f_0(\eta) &= S + \eta + \left(\frac{A_2(\varepsilon-1)}{A_1\delta + A_2}\right) \\ &\quad (1 - \exp(-\eta)) \end{aligned}\right\} \tag{31}$$

3.1 Numerical Validation

Using the Maple 18 symbolic package, we implement the SQLM iterative scheme. To express the accuracy of our code validity, we extract the skin friction coefficient values ($Re_x^{1/2} C_f$) using the SQLM iterative scheme for limiting cases available in the literature. Table 3 compares the value of $Re_x^{1/2} C_f$ when $M = Ec = S = \delta = 0$, $m = 1$, and $Pr = 6.2$ for varying values of velocity ratio parameter, ε and nanoparticle volume fraction, φ_{n_2} with the results of [3], [20], and our results agree with theirs, in Table 3. This establishes the correctness of the method and validates the results presented.

Table 3. Comparison of the SQLM results for $Re_x^{1/2} C_f$ with [3], [20], for the following values: $M = Ec = S = \delta = 0$, $m = 1$, and $Pr = 6.2$ for varying values of ε and φ_{n_2} In the case of Cu/water nanofluid $\varphi_{n_1} = 0.1$)

$Re_x^{1/2} C_f$				
ε	φ_{n_2}	[3]	[20]	Present
-0.5	0.1	2.2865	2.286512	2.28651169
-0.5	0.2	3.1826	3.182538	3.18253843
0	0.1	1.8843	1.884324	1.88432376
0	0.2	2.6226	2.622743	2.62274312
0.5	0.1	1.0904	1.090453	1.09045278
0.5	0.2	1.5177	1.517774	1.51777395

4 Discussion of Results

This segment is designed to address the behavior of the fluid parameters on the velocity profile ($f'(\eta)$), temperature distribution ($\theta(\eta)$), entropy generation number, Bejan number, the skin friction, and Nusselt number through plots and tables for the hybrid nanosuspension. Following, [20], here, the Prandtl number is taken as $Pr = 6.2$ during our discussion.

In Table 4, a comparative analysis of the Nusselt number in both Cu/water nanofluid and Cu-Al_2O_3/water hybrid nanofluid is exposed to demonstrate the effective thermal features of the hybrid nano-liquid. We observed from the result presented in Table 4 that an improvement in the heat transfer coefficient is captured for hybrid

nanofluids. In addition, Table 5 (Appendix) presents the values of the skin friction coefficient ($Re_x^{1/2}C_f$) and Nusselt number $Re_x^{-1/2}Nu_x$ for varying the nanofluid flow parameters. $Re_x^{1/2}C_f$ and $Re_x^{-1/2}Nu_x$ are enhanced with increasing values of ϕ_{n_2}, m, S, and M. However, with increasing value of H, $Re_x^{1/2}C_f$ decreases and $Re_x^{-1/2}Nu_x$ increases. Similar behavior is noticed for the case when $\varepsilon > 0$. Also, $Re_x^{-1/2}Nu_x$ is an increasing function of Ec.

Table 4. Nusselt number for Cu/ethylene gylcol and Cu-Al_2O_3/water when $m = M = Ec = S = \varepsilon = \delta = 0.5$, and $Pr = 6.2$, for various values of ϕ_{n_2}.

$Re_x^{-1/2}Nu_x$			
ϕ_{n_2}	Cu/water ($\phi_{n_1} = 0$)	Cu-Al_2O_3/water ($\phi_{n_1} = 0.1$)	% difference
0.001	3.10125361	3.32810096	7.31
0.005	3.11135376	3.34032291	7.36
0.01	3.12405619	3.35565937	7.41
0.03	3.17567132	3.41765319	7.62
0.1	3.36535206	3.64289688	8.25

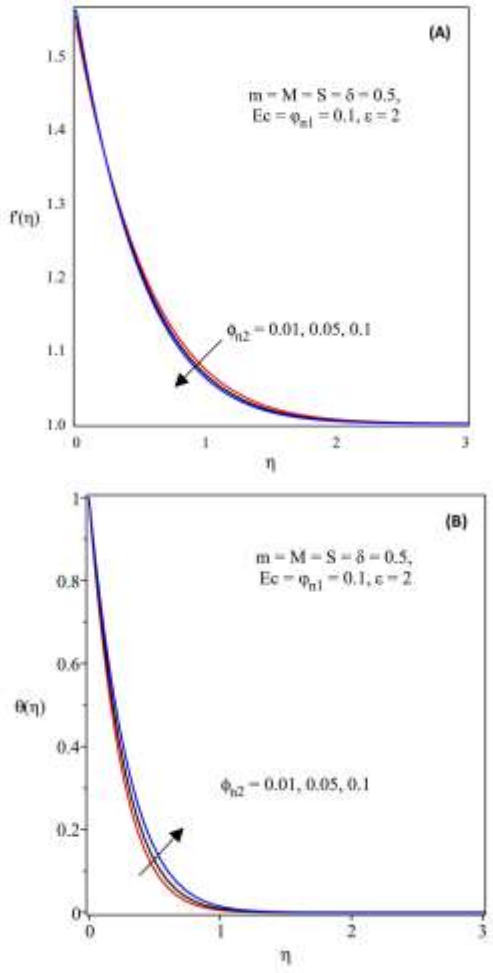

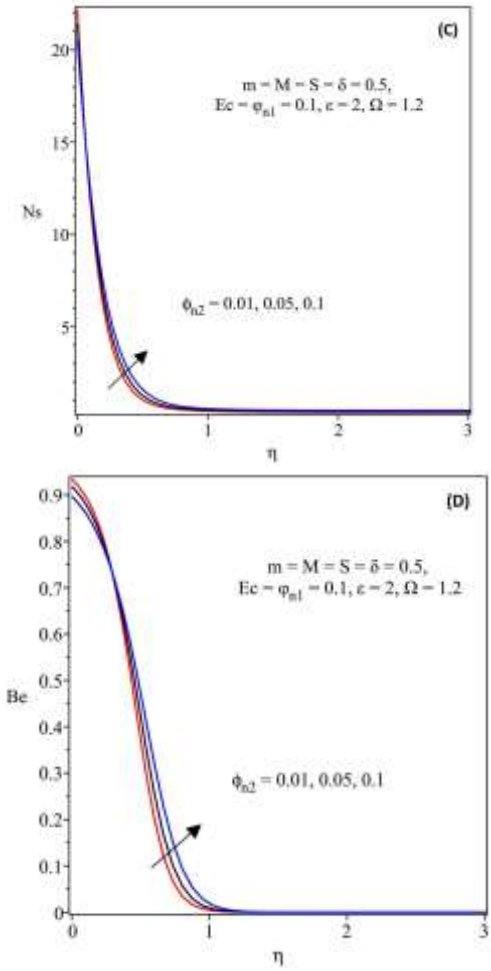

Fig. 2: Effect of varying the nanoparticle volume fraction (ϕ_{n_2}) on the hybrid nanofluid on (A) velocity profiles, (B) temperature profiles, (C) entropy generation rate, and (D) Bejan number.

Figure 2 shows the flow characteristics for rising values of nanoparticle volume fraction ϕ_{n2} for the hybrid nano-liquid. Figure 2(A-B) depicts the flow rate, heat transfer, entropy generation, and irreversibility ratio profiles, respectively for various values ϕ_{n2}. The volume fraction represents the ratio of the constituent volume of Cu-Al_2O_3/water to all constituent volume mixtures. As observed, the velocity field (Figure 2A) drops as the nanomaterial volume fraction is enhanced. This is because the overall constituent volume mixtures control the reaction as the hybrid nanofluid reduces in the stretching boundless domain. Also, we observed that the momentum boundary layer encourages convective heat transfer that leads to strengthening in the liquid bonding force; hence, the flow is dragged thereby causing a reduction in the velocity profile. Meanwhile, the heat distribution is enhanced as the nanomaterial volume fraction ϕ_{n2} is raised as presented in Figure 2B.

The rise in the temperature field is due to an increase in the thermal conducting strength of the nanoparticle, which encourages conduction and convective heat transfer within the reactive mixture. As such, the thermal boundary layer is enhanced to reduce heat diffusion, thereby causing a rise in the temperature magnitude of the system. Hence, the temperature distribution is upsurged, as observed in the profiles. In Figures 2C and 2D, the magnitude of the irreversibility and Bejan number increases as the parameter ϕ_{n2} varies. Close to the permeable stretching sheet, significant rises in both entropy generation rate and Bejan fields is noticed due to the respective dominance of fluid viscosity, Joule heating, and viscous dissipation as well as heat transfer. However, a little distance away from the plate, the irreversibility and irreversibility ratio reduce gradually towards the far stream as the dissipation of energy decreases. Therefore, entropy generation and Bejan number are minimized for the hybrid nano-liquid reactive mixture as energy loss diminishes. Hence, the nanoparticle volume fraction ϕ_{n2} reduces the energy loss far away from the porous moving plate.

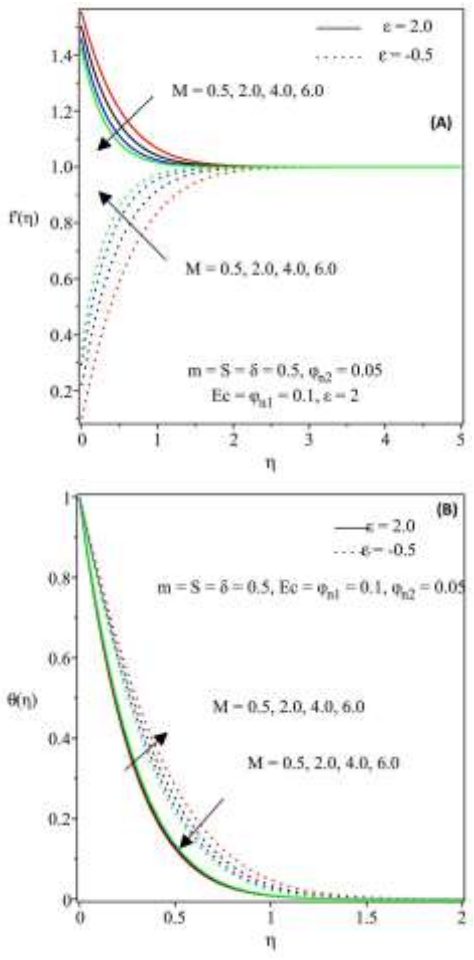

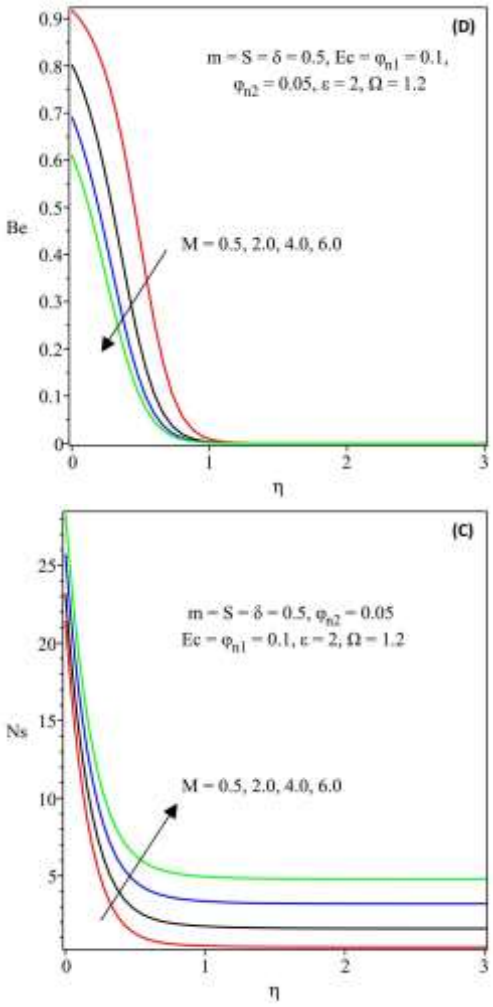

Fig. 3: Effect of varying the magnetic parameter (M) on the hybrid nanofluid on (A) velocity profiles, (B) temperature profiles, (C) entropy generation rate, (D) Bejan number

The reaction of hybrid nanofluid to rising values of a magnetic field M for the flow thermo-physics properties is displayed in Figure 3. For the value of $\varepsilon = -0.5$ or $\varepsilon = 2.0$, a respective momentous increase or decrease in the flow velocity is seen in Figure 3A. The respective flow behaviour is a result of the boost or diminishment in the heat source terms and nanoparticle thermal conductivity that leads to the breaking or strengthening of the fluid bonding force. Figure 3B shows the response of the temperature field to changes in the parameter M for different values of the velocity ratio parameter ϵ. The heat distribution for a stagnation hybrid nano liquid decreases significantly for $\varepsilon < 0$ but gradually increases for $\varepsilon > 0$ for an increasing value of M. The internal heat generation is discouraged for velocity ratio $\epsilon < 0$ which leads to a reduction in the heat distribution. Meanwhile, internal heat is raised for

velocity ratio $\varepsilon > 0$ though with little effect on the hybrid nanoparticle reactive mixtures. The heat transfer due to viscous heating is boosted all over the flow region as the magnetic field parameter M is enhanced in Figure 3C. The magnitude of entropy generated due to irreversibility is increased as a result of energy lost to the surrounding environment close to the permeable surface. Irreversibility decreases momentarily for rising magnetic fields along the free stream as distance away from the permeable surface decreases and heat dissipation to the surrounding area decreases. However, in Figure 3D, the irreversibility ratio (Bejan number) due to heat transfer diminishes, which enhances the dominance of fluid viscosity and viscous heating. Therefore, the Bejan number profile reduces as the thermal boundary layer becomes thinner, which causes more heat dissipation into the environment from the hybrid nanofluid mixture. Hence, the irreversibility ratio field is discouraged, as presented in Figure 3D, as heat diffuses out of the mixtures.

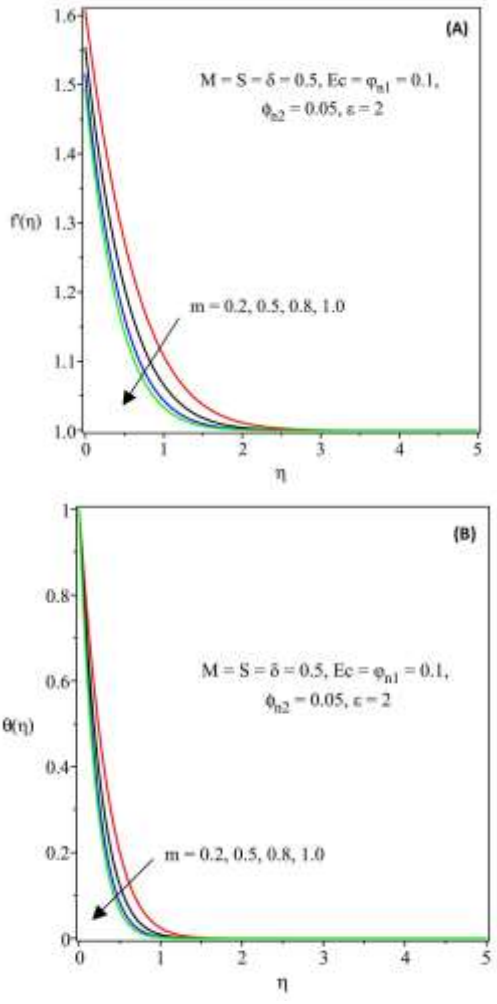

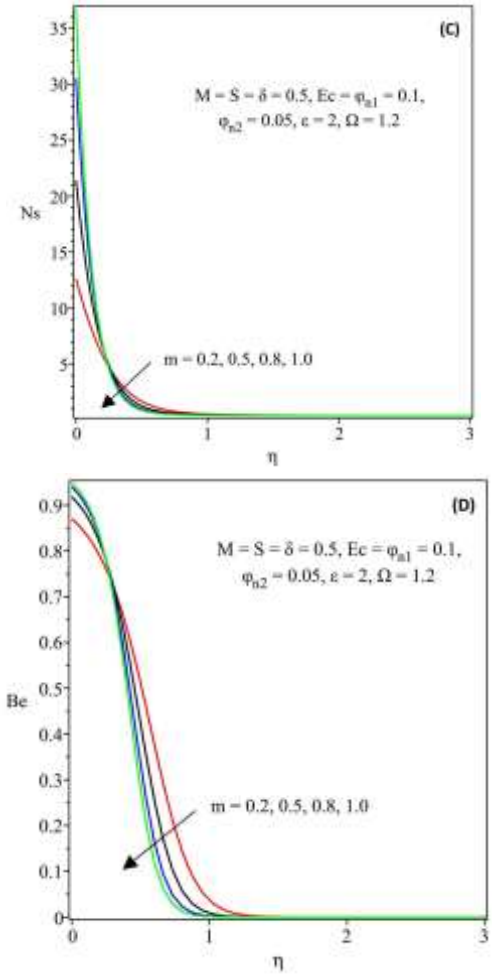

Fig. 4: Effect of varying the nonlinearity parameter (m) on the hybrid nanofluid on (A) velocity profiles, (B) temperature profiles, (C) entropy generation rate, (D) Bejan number.

Figure 4 represents the reaction of the hybrid nano liquid flow system behaviour to rising values of the non-linearity term m. The overall flow characteristics are significantly influenced by the non-linearity term, as noticed in Figure 4. In Figures 4A and 4B, the magnitude of the flow velocity and heat distribution reduce momentously for the considered Cu-Al_2O_3/water mixture. This behaviour is due to the low internal heat generation and heat conductivity of the nanoparticle, which leads to damping in the flow rate and heat transfer of the reacting mixture. Hence, the non-linearity term declines the stagnation of the hybrid nanofluid mixture. Meanwhile, in Figures 4C and 4D, the non-linearity term causes an early increase in the entropy generation and Bejan number near the permeable moving sheet. However, at a few distances from the sheet, the entropy generation and Bejan number diminish due to low heat dissipation and energy loss in the reacting nano-liquid mixture.

The continuous minimization in the irreversibility and Bejan numbers is observed in the free flow until no energy or heat is lost to the surroundings. The drastic reduction in the irreversible process enhances the optimal efficiency of the hybrid nano-liquid. This is because the thermal conductivity strength of the nanoparticle is boosted. Therefore, the irreversibility profile and irreversibility ratio decrease.

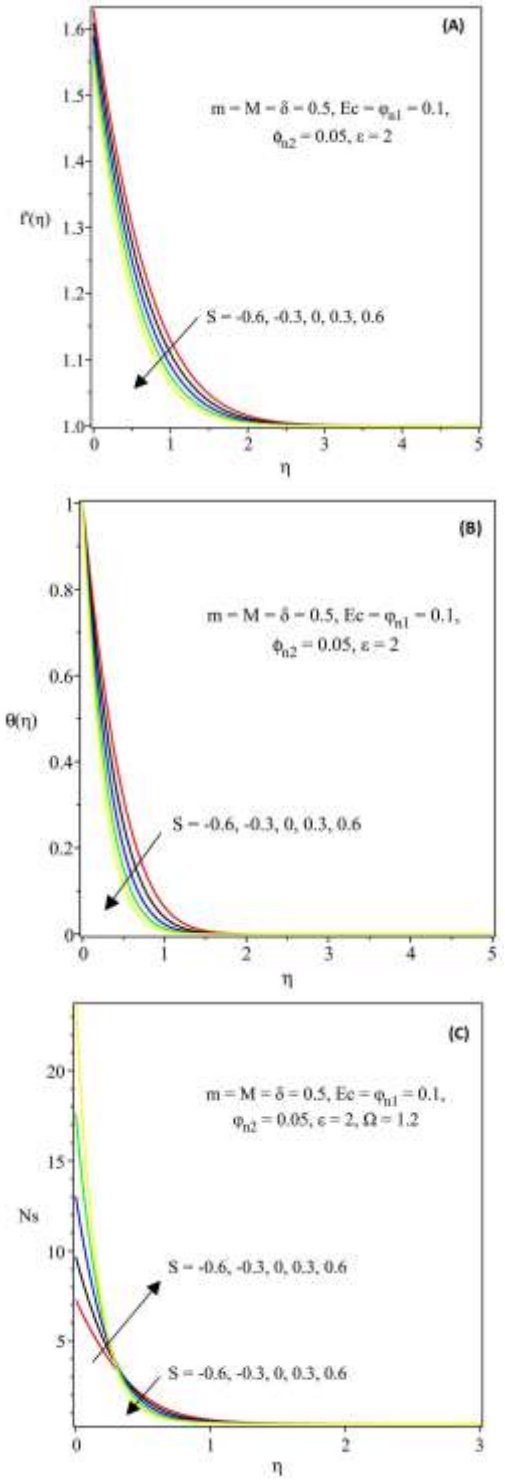

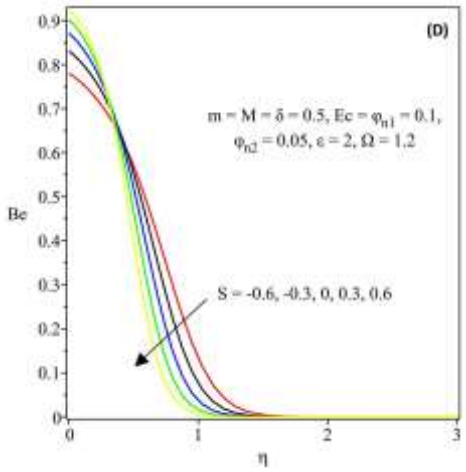

Fig. 5: Effect of varying the suction/injection parameter (S) on the hybrid nanofluid on (A) velocity profiles, (B) temperature profiles, (C) entropy generation rate, (D) Bejan number.

The impact of the suction or injection term (S) on the hybrid nanomaterial properties is demonstrated in Figure 5. As seen in Figures 5A and 5B, the velocity and temperature fields are discouraged by rising values of the parameter (S). The noteworthy declination (S) is a result of thinner momentum and heat boundary layers that dampen heat source terms and allow more heat to leave the reactive mixture. A rise in heat diffusion strengthens the hybrid nanoparticle bonding force that thereby drags the hybrid Cu-Al_2O_3/mixture. Thus, the reactive mixture flow velocity reduces in the system. More also, increasing heat lost to the ambient reduces the amount of heat within the vertical moving plate; as such, the temperature profile declines as depicted in Figure 5B. The suction effect on the hybrid nanofluid irreversibility and its ratio is examined in Figures 5C and 5D. An early rise in irreversibility is noticed due to the dominance of the nanofluid viscosity and viscous dissipation. However, after a while, the nanoparticle heat transfer rate reduces as a result of declining energy loss, which in turn decreases the entropy generation rate and irreversibility ratio. The hybrid nanofluid entropy generation and Bejan field are discouraged as the suction/injection term is raised. Therefore, the nanomaterial thermal conductivity is enhanced, which leads to increasing performance of the hybrid Cu- Al2O3/material mixture.

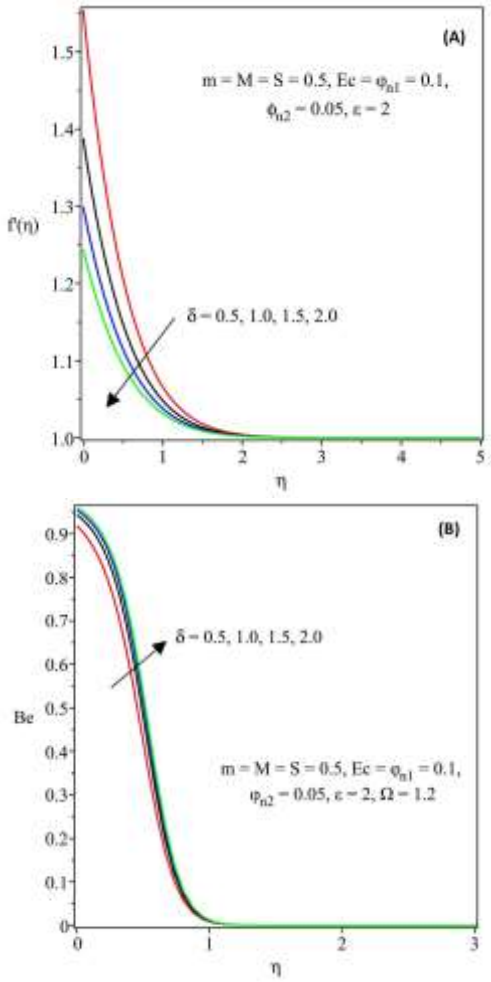

Fig. 6: Effect of varying the velocity slip parameter (δ) on the hybrid nanofluid on (A) velocity profiles, (B) Bejan number.

Figure 6 represents the reaction of the flow velocity and Bejan number to variation in the slip velocity term (H). In Figure 6A, the flow rate decreases due to very low internal heat production in the Cu-Al_2O_3 reactive mixture, which leads to an enhancement in the particle bonding force. Hence, the nanofluid velocity distribution is dragged as the fluid particles are restricted from free collision. Meanwhile, the Bejan number profile is raised for the reactive mixture because irreversibility due to heat transfer controls the hybrid nano-liquid mixture. However, the colloidal suspension irreversibility mixture decreases towards the free flow until the irreversibility vanishes away in the system, as depicted in Figure 6B. Hence, the Bejan number reduces as slip velocity is increased.

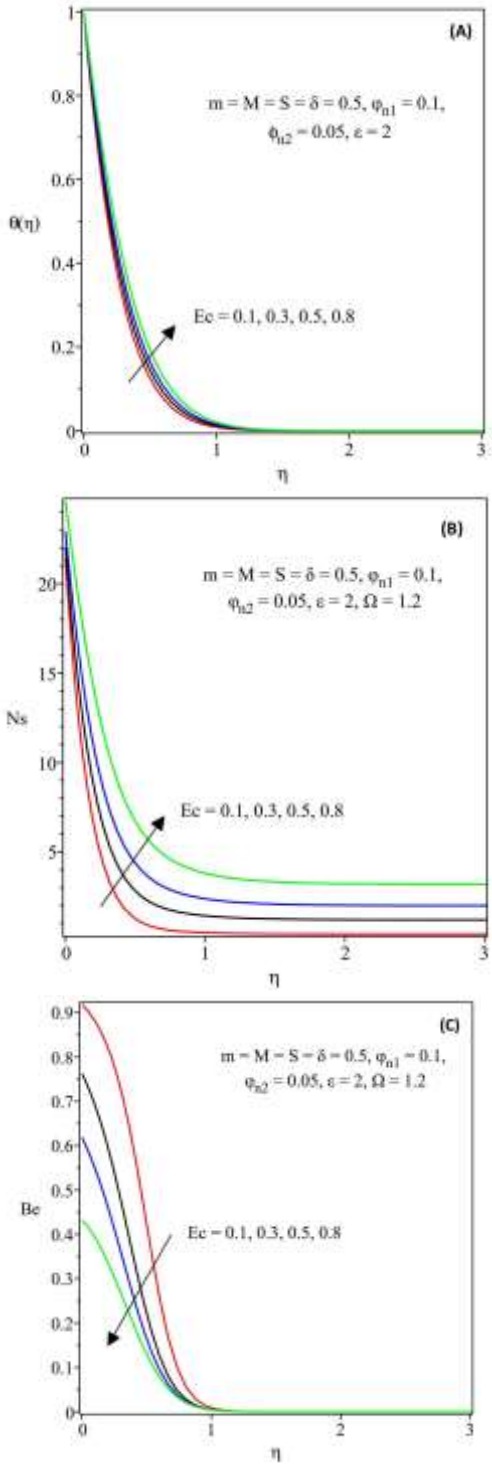

Fig. 7: Effect of varying the Eckert number (Ec) on the hybrid nanofluid on (A) temperature profiles, (B) entropy generation rate, (C) Bejan number.

The influence of Eckert number (Ec) on the hybrid nanofluid temperature field, entropy generation, and Bejan number is demonstrated in Figure 7. Eckert number is characterized by dissipative heat transport in a system; it denotes the correlation between the enthalpy boundary layer difference and the considered nanofluid kinetic

energy. Enhancing the term Ec in the chemical reaction of hybrid nano liquid steadily increases the nanoparticles' kinetic energy, which raised the particles' collision rate and then encourages temperature distribution. Therefore, the ratio of advective transport to dissipative heat potential rises, thereby causing the magnitude of heat transfer to increase, hence the temperature profile rises as denoted in Figure 7A. The entropy generation due to irreversibility and its ratio is illustrated in Figures 7B and 7C. In Figure 7B, the dissipated kinetic energy ratio to the conducted thermal energy increases as the Eckert number is boosted, this leads to a high irreversible rate in the Cu- Al2O3/mixture. Hence, the entropy generation is increased. Irreversibility due to chemical reaction controls the reactive mixture, as seen in Figure 7C. A rise in the dissipative term Ec decreases the Bejan number field due to strengthening in the hybrid nano liquid reaction mixture and a decrease in irreversibility due to friction and thermal energy. Therefore, the heat transfer irreversibility reduces, thereby causing a decrease in the Bejan number profile.

5 Conclusion

The study described the entropy generation analysis on a steady incompressible flow featuring hybrid nanofluids over a stretched permeable surface using a stable and consistent numerical scheme. The impact of pertinent factors on the flow field, thermal field, rate of entropy generation, and Bejan number is communicated through graphs for the hybrid nanosuspension to discuss the hydrothermal variations. The key outcomes of the present analysis are highlighted as follows:

- Enhanced values of the nonlinearity parameter cause a diminution of the flow and thermal distributions.
- The hybrid nanofluid possesses low skin friction for the nonlinearity parameter, whereas it augments for increasing values of the slip parameter.
- As the values of the nanoparticle volume fraction increase, the heat transfer rate is augmented to about 0.49% at the plate surface.
- The entropy generation rate upsurges with a rise in the values of the magnetic field parameter and the volume fraction parameter, while it peters out for the nonlinearity parameter.
- The employed method demonstrates excellent potential with respect to accuracy and convergence for simulating flow over stretched surfaces.

Due to the significance of the study in thermal engineering, an extension of the investigation is encouraged. As such, this work can be extended to the flow through an annular cylinder in the presence of Arrhenius kinetic and nonlinear radiation.

References:

[1] M. Bilal, A. Saeed, T. Gul, I. Ali, W. Kumam, P. Kumam, Numerical approximation of microorganisms hybrid nanofluid flow induced by a wavy fluctuating spinning disc, *Coatings*, 9(11) (2021), 1032.

[2] S. O. Salawu, A. M. Obalalu, E. O. Fatunmbi, MD Shamshuddin, Elastic deformation of thermal radiative and convective hybrid SWCNTAg and MWCNT-MoS4 magneto-nanofluids flow in a cylinder, *Results in Materials*, 17 (2023), 100380.

[3] A. Ishak, N. Bachok, I. Pop, Stagnation-point flow over a stretching/shrinking sheet in a nanofluid, *Nanoscale Research Letters*, (2011), 623.

[4] T. Gul, M.A. Khan, W. Noman, I. Khan, T.A. Alkanhal, I. Tlili, Fractional order forced convection carbon nanotube nanofluid flow passing over a thin needle, *Symmetry*, 11(3) (2019), 312.

[5] S.O. Salawu, A.M. Obalalu, S.S. Okoya, Thermal convection and solar radiation of electromagnetic actuator Cu-Al2O3/C3H8O2 and Cu-C3H8O2 hybrid nanofluids for solar collector optimization, *Materials Today Communications* 33 (2022), 104763.

[6] B. Jalili, S. Sadighi, P. Jalili, D.D. Ganji, Characteristics of ferrofluid flow over a stretching sheet with suction and injection, *Case Studies in Thermal Engineering*, 14 (2019), 100470

[7] S.O. Salawu, R.A. Oderinu, A.D. Ohaegbue, Thermal runaway and thermodynamic second law of a reactive couple stress hydromagnetic fluid with variable properties and navier slips, *Scientific African*, 7 (2020), e00261.

[8] H.A. Ogunseye, S.O. Salawu, S.D. Oloniiju, M.T. Akolade, Y.O. Tijani, R. Mustapha, P. Sibanda, MHD Powell-Eyring nanofluid motion with convective surface condition and Dufour-Soret impact past a vertical plate: Lie

group analysis, *Partial Differential Equations in Applied Mathematics*, 6 (2022), 100459.

[9] H.A. Ogunseye, Y.O. Tijani, P. Sibanda, Entropy generation in an unsteady eyring-powell hybrid nanofluid flow over a permeable surface: A lie group analysis, *Heat Transfer*, 10 (2020), 21778.

[10] B. Jalili, A.D. Ganji, P. Jalili, S.S. Nourazzar, D.D. Ganji, Thermal analysis of Williamson fluid flow with Lorentz force on the stretching plate, *Case Studies in Thermal Engineering*, 39 (2022), 102374

[11] D. Lu, M. Ramzan, M. Mohammad, F. Howari, J.D. Chung, A thin film flow of nanofluid comprising carbon nanotubes influenced by cattaneo-christov heat flux and entropy generation, *Coatings*, 9(5), (2019), 9050296.

[12] S.U.S. Choi, J.A. Eastman, Enhancing thermal conductivity of fluids with nanoparticles, *Proceedings of the ASME International Mechanical Engineering Congress and Exposition*, 66, (1995) p.687-694.

[13] S.U.S. Choi, W. Yu, S.K. Das, T. Pradeep, Nanofluids, Science and technology, John Wiley & Sons, Inc, (2008).

[14] S. Qayyum, I.M. Khan, T. Hayat, A. Ahmed, Comparative investigation of five nanoparticles in flow of viscous fluid with joule heating and slip due to rotating disk, *Physica B: Condensed Matter*, 534, (2018), p.173–183.

[15] S.O. Salawu, R.A. Kareem, J.O. Ajilore, Eyring-Powell MHD nanoliquid and entropy generation in a porous device with thermal radiation and convective cooling, *J. of the Nigeria Society of Physical Sciences*, 4, (2022), p.924.

[16] S.U. Devi, S.A. Devi, Heat transfer enhancement of Cu-Al2O3/water hybrid nanofluid flow over a stretching sheet, *J. of the Nigerian Mathematical Society*, 36, (2017), p.419-433.

[17] T. Hayat, S. Nadeem, Heat transfer enhancement with Ag-CuO/water hybrid nanofluid, *Results in Physics*, 7, (2017), p.2317–2324.

[18] T. Hayat, F. Haider, T. Muhammad, A. Alsaedi, Darcy-forchheimer three dimensional flow of carbon nanotubes with nonlinear thermal radiation, *J. of Thermal Analysis and Calorimetry*, 140, (2020) s10973.

[19] P. Jalili, A.A. Azar, B. Jalili, Z. Asadi, Heat transfer analysis in cylindrical polar system with magnetic field: A novel hybrid analtical and numerical technique, *Case Study in Thermal Engin*., 40 (2022), 102524.

[20] A. Ishak, I. Waini, I. Pop, MHD flow and heat transfer of a hybrid nanofluid past a permeable stretching/shrinking wedge, *Applied Mathematics and Mechanics*, 41 (2020), p.507-520.

[21] M. Ramzan, S. Riasat, C.J. Dong, Y.M. Chu, M. Sheikholeslami, S. Kadry, F. Howari, Upshot of heterogeneous catalysis in a nanofluid flow over a rotating disk with slip effects and entropy optimization analysis, *Scientific Reports*, 11 (2021), s41598.

[22] B. Jalili, N. Aghaee, P. Jalili, D.D. Ganji, Novel usage of the curved rectanglar fin on the heat transfer of a double-pipe heat exchanger with a nanofluid, *Case Study in Thermal Engin*., 35 (2022), 102086.

[23] S.O. Salawu, Two-step exothermic reaction-diffusion of hydromagnetic Prandtl-Eyring viscous heating fluid in a channel, *Int. J. of Thermofluids*, 17 (2023), 100300.

[24] M.I. Khan, S. Qayyum, S. Kadry, W.A. Khan, S.Z. Abbas, Irreversibility analysis and heat transport in squeezing nanoliquid flow of non-newtonian (second-grade) fluid between infinite plates with activation energy, *Arabian Journal for Science and Engineering*, 45 (2020), p.4939–4947.

[25] A. Shahsavar, P.T. Sardari, D. Toghraie, Free convection heat transfer and entropy generation analysis of water-fe3o4/cnt hybrid nanofuid in a concentric annulus, *Int. J. of Numerical Methods for Heat & Fluid Flow*, 29(4) (2019), p.2018-2024.

[26] S. Ahmad, S. Nadeem, N. Ullah, Entropy generation and temperature dependent viscosity in the study of swcntâĂŞmwcnt hybrid nanofuid, *Applied Nanoscience*, 13 (2020), s13204.

[27] Yusuf, T. A., R. Ukaegbu, J.C., and Ayinde, A.M., Irreversibility analysis in thehydrothermal flow of $\gamma Al_2O_3/H_2O$ and $\gamma Al_2O_3/C_2H_6O_2$ over a permeable stretching surface with effective Prandtl number, *Waves in Random and Complex Media*, (2022), https://doi.org/10.1080/17455030.2022.2155323

[28] P. Jalili, A.S. Ghahare, B. Jalili, D. D. Ganji, Analytical and numerical investigation of thermal distribution for hybrid nanofluid

through an oblique artery with mild stenosis, *SN Applied Sci*., 95 (2023), s42452.

[29] S.O. Salawu, A.M. Obalalu, MD. Shamshuddin, Nonlinear solar thermal radiation efficiency and energy optimization for magnetized hybrid Prandtl-Eyring nanoliquid in aircraft. *Arabian J. for Sci. and engin*., 22 (2022), 070801.

[30] S.S. Motsa, A new spectral local linearization method for nonlinear boundary layer flow problems, *J. of Applied Mathematics*, 13 (2013), 423628.

[31] H.A. Ogunseye, E.O. Fatunmbi, P. Sibanda, Magnetohydrodynamic micropolar fluid flow in a porous medium with multiple slip conditions, *Int. Commun. in Heat and Mass Transfer*, 115 (2020), 104577.

[32] R.E. Bellman, R.E. Kalaba, *Quasilinearization and nonlinear boundary-value problems*, (1965).

[33] L.N. Trefethen, *Spectral methods in MATLAB*, Siam, 10 (2000).

Appendix

Table 5. The statistical data for the skin friction coefficient and Nusselt number for Cu-Al $_2$O $_3$/water ($\phi_{n_1} = 0.1$) hybrid nanofluid

ϕ_{n_2}	m	M	S	ε	δ	Ec	$-Re_x^{1/2}C_f$	$Re_x^{-1/2}Nu_x$
0.001	0.5	0.5	0.5	2	0.5	0.5	1.204108576	3.315391243
0.005	0.5	0.5	0.5	2	0.5	0.5	1.220313025	3.328393413
0.01	0.5	0.5	0.5	2	0.5	0.5	1.240694846	3.344756145
0.1	0.2	0.5	0.5	2	0.5	0.5	1.642556027	3.659691749
0.1	0.5	0.5	0.5	2	0.5	0.5	1.098739958	1.073055261
0.1	0.8	0.5	0.5	2	0.5	0.5	1.240694846	3.344756145
0.1	1	0.5	0.5	2	0.5	0.5	1.342452049	4.810744382
0.1	0.5	0.5	0.5	2	0.5	0.5	1.397090086	5.609892787
0.1	0.5	0	0.5	2	0.5	0.5	1.17458904	5.007446213
0.1	0.5	0.3	0.5	2	0.5	0.5	1.215708203	3.999445799
0.1	0.5	0.5	0.5	2	0.5	0.5	1.240694846	3.344756145
0.1	0.5	0.8	0.5	2	0.5	0.5	1.275110522	2.384597808
0.1	0.5	0.5	-0.5	2	0.5	0.5	1.066719419	1.648327654
0.1	0.5	0.5	-0.3	2	0.5	0.5	1.101391086	1.906004528
0.1	0.5	0.5	0	2	0.5	0.5	1.153722426	2.369501198
0.1	0.5	0.5	0.3	2	0.5	0.5	1.206039213	2.925282015
0.1	0.5	0.5	0.5	2	0.5	0.5	1.240694846	3.344756145
0.1	0.5	0.5	0.5	-0.5	0.5	0.5	1.662773645	1.612424622
0.1	0.5	0.5	0.5	-0.3	0.5	0.5	1.459327908	2.098984483
0.1	0.5	0.5	0.5	1	0.5	0.5	1.46244E-07	3.664105655
0.1	0.5	0.5	0.5	1.5	0.5	0.5	0.609911794	3.652495598
0.1	0.5	0.5	0.5	2	0.5	0.5	1.240694846	3.344756145
0.1	0.5	0.5	0.5	0.5	0.1	0.5	2.034448487	2.592949542
0.1	0.5	0.5	0.5	0.5	0.3	0.5	1.537704272	3.108090507
0.1	0.5	0.5	0.5	0.5	0.5	0.5	1.240694846	3.344756145
0.1	0.5	0.5	0.5	0.5	1	0.5	0.840924452	3.572167774
0.1	0.5	0.5	0.5	0.5	0.5	0.1	1.240694846	5.038423866
0.1	0.5	0.5	0.5	0.5	0.5	0.3	1.240694844	4.191590005
0.1	0.5	0.5	0.5	0.5	0.5	0.5	1.240694846	3.344756145
0.1	0.5	0.5	0.5	0.5	0.5	0.8	1.240694847	2.074505355

Contribution of Individual Authors to the Creation of a Scientific Article (Ghostwriting Policy)

All authors equally contributed in the present research, at all stages from the formulation of the problem to the final findings and solution.

Data Availability

Data sharing not applicable to this article as no datasets were generated or analysed during the current study

Sources of Funding for Research Presented in a Scientific Article or Scientific Article Itself

No funding was received for conducting this study.

Conflict of Interest

The authors have no conflict of interest to declare.